Unoccupied topological surface state in $MnBi_2Te_4$

Yadong Jiang,[1] Zhaochen Liu,[1] and Jing Wang[1,2,3,*]

[1]*State Key Laboratory of Surface Physics and Department of Physics, Fudan University, Shanghai 200433, China*
[2]*Institute for Nanoelectronic Devices and Quantum Computing, Fudan University, Shanghai 200433, China*
[3]*Zhangjiang Fudan International Innovation Center, Fudan University, Shanghai 201210, China*

(Received 16 November 2021; revised 8 June 2022; accepted 20 July 2022; published 29 July 2022)

The unoccupied part of the band structure in the magnetic topological insulator $MnBi_2Te_4$ is studied by first-principles calculations. We propose a possible second, unoccupied topological surface state with a similar electronic structure to the celebrated occupied topological surface state. The conventional density functional theory method employed here may not describe excited state properties precisely, and therefore the calculations for the current study can be considered as model simulations. This unoccupied topological surface state is energetically located approximate 1.5 eV above the occupied massive Dirac surface state around the Γ point, which permits it to be directly observed by two-photon angle-resolved photoemission spectroscopy. We propose a unified effective model for the occupied and unoccupied surface states. Due to the direct optical coupling between these two surface states, we further propose two optical effects to detect the unoccupied surface state if it exists. One is the polar Kerr effect in odd layers from nonvanishing ac Hall conductance $\sigma_{xy}(\omega)$, and the other is higher-order terahertz-sideband generation in even layers, where the nonvanishing Berry curvature of the unoccupied surface state is directly observed from the giant Faraday rotation of optical emission.

DOI: 10.1103/PhysRevB.106.045148

I. INTRODUCTION

Topology has become one of the central topics in condensed matter physics [1–9]. A prime example is the topological insulators (TI), which are characterized by an insulating bulk, and the hallmark Dirac surface states (SS) protected by time-reversal symmetry [10–13]. The linearly dispersing SS has a chiral spin texture with a nontrivial Berry phase, which is promising for spintronics applications [14,15]. A number of interesting phenomena are associated with the symmetry breaking of SS in TI, such as quantum anomalous Hall effect [16–18], quantized Kerr rotation [19–24], and image magnetic monopole [25] in magnetic TI, as well as Majorana fermion in the presence of superconductors [26].

Most of these phenomena are focused on low-energy electronic excitations. There are also quite a few works studying the excited electronic states and their dynamics in TI [27–31]. An interesting example is the discovery of unoccupied SS in Bi_2Se_3, which has a similar electronic structure and physical origin to the occupied topological SS [29,30]. Recently an intrinsic magnetic TI $MnBi_2Te_4$ has been discovered [32–40]. The material consists of van der Waals coupled Te-Bi-Te-Mn-Te-Bi-Te septuple layers (SL) arranged along a trigonal z axis, so it can be viewed as layered TI Bi_2Te_3 with each of its Te-Bi-Te-Bi-Te quintuple layers intercalated by an additional Mn-Te bilayer. The resultant $MnBi_2Te_4$ remains a TI but now becomes intrinsically magnetic, where the hallmark first topological SS has been observed [34–39]. The intimate relation between the $MnBi_2Te_4$ and Bi_2Te_3 family motivates us to study the topological properties of higher-excited electronic states in $MnBi_2Te_4$.

In this paper, we propose a possible second, unoccupied topological SS in $MnBi_2Te_4$ suggested by first-principles calculations. It has a similar physical origin but is energetically located 1.5 eV above the well-known occupied SS. The density functional theory method employed here may not describe excited state properties precisely, and therefore the calculations of the current study can be considered as model simulations. We assume that the second SS exist, and further propose that the direct optical coupling between the occupied and unoccupied SS permits it to be directly observed by two-photon photoemission (2PPE) and higher-order terahertz-sideband generation (HSG).

The organization of this paper is as follows. Section II describes the band structure calculations, parity analysis, and second SS. Section III describes the unified effective model for both the first and second SS. Section IV presents several experimental proposals to detect the second SS, if it exists. Section V concludes this paper. Some auxiliary materials are relegated to the Supplemental Material [41].

II. BAND STRUCTURE

$MnBi_2Te_4$ has a rhombohedral crystal structure with space group D_{3d}^5 (No. 166). The magnetism originates from the Mn^{2+} ions in the crystal. Below a Néel temperature of $T_N = 25$ K, the system develops A-type antiferromagnetic (AFM) order with an out-of-plane easy axis, which is ferromagnetic (FM) within each SL but AFM between adjacent SL along the z axis [32–35]. The existence of inversion symmetry $\mathcal{P}$, with

*Corresponding author: wjingphys@fudan.edu.cn

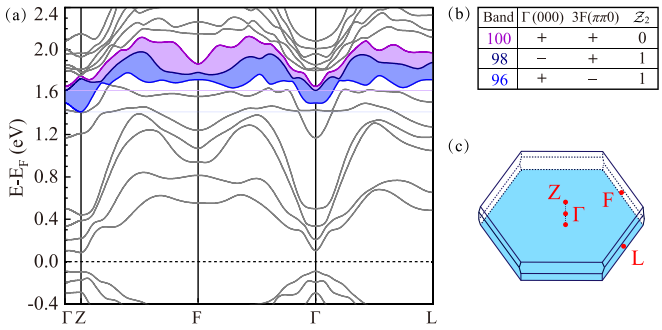

Band	Γ(000)	3F($\pi\pi$0)	$\mathcal{Z}_2$
100	+	+	0
98	−	+	1
96	+	−	1

FIG. 1. (a) Electronic structure of AFM-z ground state in $MnBi_2Te_4$. The topologically nontrivial unoccupied bands are colored. All energy bands have twofold degeneracy due to $\mathcal{S}$ and $\mathcal{P}$ symmetry. (b) The parity product of the unoccupied bands at the TRIM with $\bar{\mathbf{G}} \cdot \tau_{1/2} = n\pi$. (c) Brillouin zone. The four inequivalent TRIM are $\Gamma(000)$, $L(\pi 00)$, $F(\pi\pi 0)$, and $Z(\pi\pi\pi)$.

the Mn site as the inversion center, enables us to construct eigenstates with definite parity.

A. Parity analysis

First-principles calculations are employed to investigate the electronic structure of $MnBi_2Te_4$, where the detailed methods can be found in the Supplemental Material [41–57]. The calculations were based on the experimentally determined crystal structure [35], with the in-plane lattice constant from the experiment fixed throughout the calculations [41]. The AFM-z ground state breaks the time-reversal symmetry Θ; however, a combined symmetry $\mathcal{S} = \Theta\tau_{1/2}$ is preserved, where $\tau_{1/2}$ is the half translation operator connecting adjacent spin-up and -down Mn atomic layers. Here the operator $\mathcal{S}$ is antiunitary with $\mathcal{S}^2 = -e^{-i\mathbf{k}\cdot\tau_{1/2}}$, and $\mathcal{S}^2 = -1$ on the Brillouin zone (BZ) plane $\mathbf{k} \cdot \tau_{1/2} = 0$. Therefore, similar to Θ in time-reversal invariant TI, $\mathcal{S}$ could also lead to a $\mathcal{Z}_2$ classification [58], where the topological invariant is only well defined on the BZ plane with $\mathbf{k} \cdot \tau_{1/2} = 0$. Since $\mathcal{P}$ is preserved, the $\mathcal{Z}_2$ invariant is simply the parity of the wave functions of all occupied bands at time-reversal-invariant momenta (TRIM) in the BZ proposed by Fu and Kane [59]. Here we only need to consider four TRIM (Γ and three F) with $\bar{\mathbf{G}} \cdot \tau_{1/2} = n\pi$.

Previous studies have revealed the nontrivial $\mathcal{Z}_2$ invariant for all occupied bands [32,33], which signifies the first topological SS shown in Figs. 2(a) and 2(b). Here we focus on the topologically nontrivial unoccupied state above the Fermi energy. As shown in Fig. 1(a), the different parity product between Γ and F leads to $\mathcal{Z}_2 = 1$, if we put the *artificial* Fermi energy at the blue region (namely, between the 96th and 98th bands) or at the purple region (namely, between the 98th and 100th bands). Such nontrivial $\mathcal{Z}_2$ suggests the existence of unoccupied topological bands. The band inversion for the unoccupied topological states (96th and 100th bands) happens between $p^{\pm}_{x,y}$ orbitals of Bi [41], which is slightly different from the occupied topological states where the band inversion is between the p^{+}_{z} orbital of Bi and the p^{-}_{z} orbital of Te. Therefore, the second unoccupied topologically nontrivial SS, if it exists, is expected to appear between the 96th and 100th band, as shown by shade in Fig. 1(a). Moreover, we find

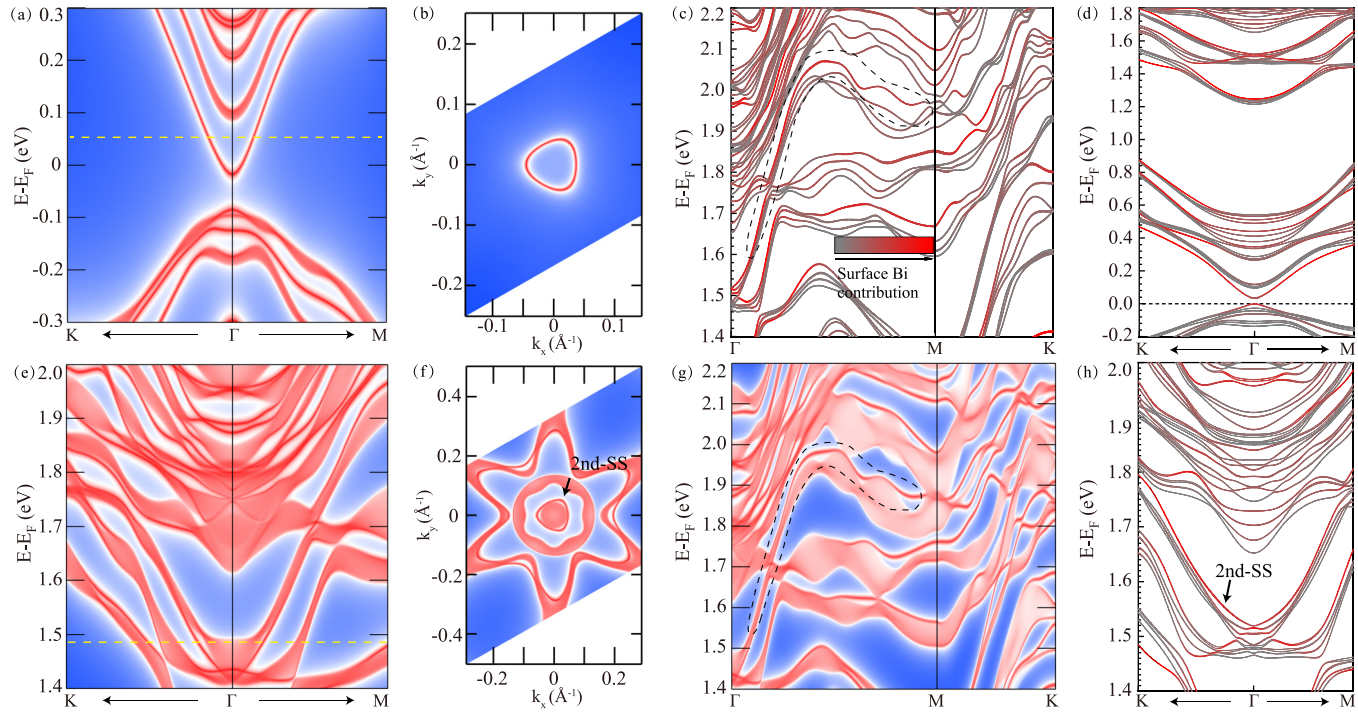

FIG. 2. Band structure calculations of SS in $MnBi_2Te_4$. (a), (e), and (g) Energy and momentum dependence of the LDOS for AFM-z state on the (111) surface based on maximally localized Wannier functions. (b) and (f) The constant energy contour for first and second SS at energy level 0.05 eV and 1.47 eV, respectively. (c) and (d) Slab band structure calculation of eight SL $MnBi_2Te_4$. The top of the valence band is set as the Fermi energy. The color of the bands represents the degree of surface localization. The SS in (c) shows a one-to-one correspondence with that in (g) as highlighted in the dashed box. (h) A magnified view of (d) with energy between 1.4 and 2.0 eV.

that both the band structure and $\mathcal{Z}_2$ invariant are insensitive to the lattice constant (±0.5% strain) as well as the choice of different van der Waals interaction functional [41]. In the following, we assume that a second SS exists in $MnBi_2Te_4$ and study its physical consequences and experimental detections.

B. Second SS

The existence of topological SS is the hallmark of TI. To explore the first and second SS, we now turn to the local density of states (LDOS) and slab calculations. It is worth mentioning that the TI state in AFM $MnBi_2Te_4$ protected by $\mathcal{S}$ is topological in a weaker sense than the strong TI protected by Θ, which manifests in that the existence of gapless SS depends on the surface plane. The first SS on the (111) surface is clearly shown in Figs. 2(a) and 2(b), which is gapped and accompanied by a triangular Fermi surface, for $\mathcal{S}$ is broken. The second SS on the (111) surface is highlighted by an arrow in Figs. 2(e) and 2(f). The second SS is buried among the bulk state along Γ-Z due to projection to the surface $\bar{\Gamma}$ point in Fig. 2(e). To better resolve the second SS from the complex electronic structure, we further display the explicit slab calculation of eight SL in Fig. 2(c) for comparison. One can identify an unambiguous one-to-one correspondence of the second SS across the entire BZ between Figs. 2(c) and 2(g). This state is energetically located approximately $1.5 - 1.9$ eV above the occupied first topological SS around the Γ point, though the energy position shifts a little in Figs. 2(c) and 2(g). As expected, the second SS is also magnetically gapped at Γ from the magnified view in Fig. 2(h). The magnetic gap of the second SS is smaller than that of the first SS, because the exchange field is from Mn^{2+} d orbitals which lie far below the Fermi level. Moreover, just like the first SS, the second SS exists only in the presence of crystal spin-orbit coupling, as suggested by calculations in Fig. 2 and Supplemental Material [41]. This suggests that both SS share the same physical origin, as they both arise due to band inversion of bulk states in the presence of strong spin-orbit coupling.

III. EFFECTIVE MODEL

We study the surface band structure near Γ using $\mathbf{k}\cdot\mathbf{p}$ theory. To lowest order in $\mathbf{k}$, the 2×2 effective Hamiltonian reads $H_0 = v(k_x\sigma_y - k_y\sigma_x) + m\sigma_z$, which describes an isotropic gapped two-dimensional (2D) Dirac fermion. The Fermi surface of H_0 is a circle at any Fermi energy. Thus the anisotropic Fermi surface for the first and second SS in Fig. 2 can only be explained by higher-order terms in the $\mathbf{k}\cdot\mathbf{p}$ Hamiltonian $\mathcal{H}(\mathbf{k})$ that breaks the emerging $U(1)$ rotational symmetry of H_0. From the constraint of crystal symmetry, C_3 around the trigonal z-axis transforms the momentum and spin as $C_3 : k_\pm \to e^{\pm i2\pi/3}k_\pm$, $\sigma_\pm \to e^{\pm i2\pi/3}\sigma_\pm$, and $\sigma_z \to \sigma_z$, where $k_\pm = k_x \pm ik_y$, $\sigma_\pm = \sigma_x \pm i\sigma_y$, and k_x is in the ΓK direction. We then find that $\mathcal{H}(\mathbf{k})$ takes the following form up to the third order in $\mathbf{k}$:

$$\mathcal{H}_i(\mathbf{k}) = E_0^i(\mathbf{k}) + v_k^i(k_y\sigma_x - k_x\sigma_y) + \frac{\lambda_i}{2}(k_+^3 + k_-^3)\sigma_z + \Delta_i\sigma_z, \tag{1}$$

where $i = 1, 2$ denotes the first and second SS, respectively; $E_0^i(\mathbf{k}) = \epsilon_0^i + k^2/2m_i^*$ generates particle-hole asymmetry; the Dirac velocity $v_k^i = v_i(1 + \alpha_i k^2)$ has a second-order correction; and λ_i is the threefold warping term similar to Bi_2Te_3 [60]. Δ_i is the exchange field along the z axis on the (111) surface introduced by magnetic ordering, which is odd under any mirror symmetry in two dimensions. The surface band dispersion of $\mathcal{H}_i(\mathbf{k})$ is

$$E_\pm^i(\mathbf{k}) = E_0^i(\mathbf{k}) \pm \sqrt{v_i^2k^2 + [m_i + \lambda_i(k_x^3 - 3k_xk_y^2)]^2}. \tag{2}$$

Here $E_\pm$ denotes the upper and lower band. The shape of the constant energy contour is energy-dependent and always forms a closed loop around Γ. Although the Hamiltonian $\mathcal{H}$ is threefold invariant, the band structure in Eq. (2) is approximately sixfold symmetric when the energy is far away from the Dirac point. In the following we propose several optical experiments to reveal the properties of the second SS.

IV. EXPERIMENTAL PROPOSALS

A. 2PPE measurement

To experimentally identify the second unoccupied SS, a direct way is to employ angle-resolved 2PPE spectroscopy. Distinct from conventional one-photon photoemission for occupied states measurement, 2PPE could access unoccupied states [29,30]. In the 2PPE process, a photon first excites an electron from below Fermi energy to an unoccupied intermediate state, and a second photon further excites the electron above the vaccum.

B. HSG in even SL

In even SL $MnBi_2Te_4$, $\mathcal{P}\Theta$ is conserved due to fully compensated magnetic layers. Therefore, the ac Hall conductance $\sigma_{xy}(\omega)$ vanishes, which further leads to vanishing linear optical Kerr or Faraday effect. In the limit of $\omega \to 0$, $\sigma_{xy}(0) = 0$ is one transport signature for an axion insulator [32,61–65], where the interesting topological magnetoelectric effect associated with the first SS is proposed [16,62,66–69]. Here we employ the extreme nonlinear optical phenomena, namely, HSG, to detect the nontrivial Berry curvature of the second SS around the Γ point. HSG could have interesting effects due to nontrivial vacuum states of materials [70–75]. Previous studies of the multivalley system such as monolayer MoS_2 have shown that the finite valley Berry curvature is revealed through HSG [72–74]. In MoS_2, two degenerate valleys related by Θ have opposite Berry curvatures and optical selection rules [76]. The quantum trajectories of optically excited electron-hole pairs in two valleys driven under an intense THz field accumulate opposite Berry phases, and the interference of optical transitions between two valleys leads to Faraday rotation of emission.

Here we show that the optical transitions of the *gapped* first SS to second SS on the top and bottom surfaces in even SL are the same as those of two valleys in MoS_2. The effective Hamiltonian for even SL is $H_i = E_0^i + v_i(k_y\sigma_x - k_x\sigma_y)\tau_z + \Delta_i\sigma_z\tau_z$, with the basis of $|t\uparrow\rangle$, $|t\downarrow\rangle$, $|b\uparrow\rangle$, and $|b\downarrow\rangle$, where t and b denote the top and bottom surfaces and $\uparrow$ and $\downarrow$ represent spin-up and -down states, respectively. $\sigma_{x,y,z}$ and τ_z are Pauli matrices for spin and layers. t and b layers are decoupled. The Bloch state is denoted as $\psi_i^\pm(\mathbf{k}) = e^{i\mathbf{k}\cdot\mathbf{r}}|i^\pm, \mathbf{k}\rangle$, where $i = 1, 2$ refers to the first and second SS, respectively,

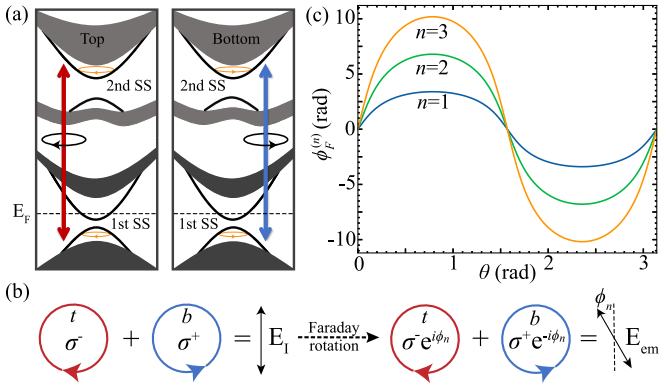

FIG. 3. (a) Schematics of HSG between the lower band of first SS and the upper band of second SS on t and b surfaces, where the optical selection rules are opposite. (b) The linear polarized light from two opposite circular polarizations $|\sigma_-\rangle + |\sigma_+\rangle$ will excite optical transitions in two layers, resulting in the coherent superposition of the electron-hole pair state $|t\rangle + |b\rangle$. The cyclic evolutions under terahertz (THz) field accumulate opposite the Berry phase $e^{i\phi_n}|t\rangle + e^{-i\phi_n}|b\rangle$, which further leads to Faraday rotation of emission $e^{i\phi_n}|\sigma_-\rangle + e^{-i\phi_n}|\sigma_+\rangle$. (c) The Faraday rotation angle $\phi_F^{(n)}$ as a function of the polarization angle θ of elliptical driving laser at $n = 1, 2, 3$. Here n is the number of completed THz period experience by the electron-hole pairs.

$+$ and $-$ denote the upper and lower band, respectively. The optical transition from the lower band of the first SS to the upper band of the second SS is in the visible range as shown in Fig. 3(a). The interband dipole moment is $\mathbf{d}_{t/b}(\mathbf{k}) = -ie\langle\psi_2^+(\mathbf{k})|\nabla_\mathbf{k}|\psi_1^-(\mathbf{k})\rangle_{t/b} \approx d_{12}(\mathbf{e}_x \mp i\mathbf{e}_y)$, i.e., the SS on t and b can be optically pumped by opposite circular polarized light. The optical selection rules remain the same even with finite hybridization between these two surfaces [41]. Also, the Berry curvatures for the second SS on t and b are opposite. The surface index in even SL magnetic TI is an exact analogy to the valley index in MoS_2.

After weak optical laser pumping $\mathbf{E}_I e^{-i\Omega t}$, the excited pairs of electron-holes reside at SS $|2^+, \mathbf{k}\rangle$ and $|1^-, \mathbf{k}\rangle$ states, respectively. The Berry phase is accumulated by varying the parameter $\mathbf{k}$ in a closed path. Now in the presence of a strong THz driving field $\mathbf{F}(t)$, minimal coupling leads to the time-dependent Hamiltonian $H[\tilde{\mathbf{k}}(t)]$ via $\tilde{\mathbf{k}}(t) \to \mathbf{k} + e\mathbf{A}(t)$, with $\mathbf{F} = -\partial\mathbf{A}/\partial t$. The instantaneous eigenstate is $H[\tilde{\mathbf{k}}(t)]|\mu, \tilde{\mathbf{k}}(t)\rangle = E^\mu_{\tilde{\mathbf{k}}(t)}|\mu, \tilde{\mathbf{k}}(t)\rangle$, where $\mu = 2^+, 1^-$ is the band index. Here the lifetime of a nonequilibrium population of the second SS is unknown and is beyond the scope of the current study. Since the second SS and first SS are similar, and if we take the experimental value of the long-lived first SS in Bi_2Se_3 persisting >10 ps [77] for the second SS in $MnBi_2Te_4$, then the electron-hole pairs accelerated by the THz field could complete several cyclic evolutions in $\mathbf{k}$ space before they scatter into bulk states. Thus we assume that the states that evolve in $\mathbf{k}$ space would follow $\tilde{\mathbf{k}}(t)$ adiabatically. The linear optical response now is

$$\mathbf{P}(t) = i\int_{-\infty}^{t} dt' \int d\mathbf{k}\mathbf{d}^*_{\tilde{\mathbf{k}}(t)}\mathbf{d}_{\tilde{\mathbf{k}}(t')} \cdot \mathbf{E}_I \, e^{-i\int_{t'}^{t}\delta E_{\tilde{\mathbf{k}}(\tau)}d\tau + i\int_{t'}^{t}\mathcal{A}_{\tilde{\mathbf{k}}(\tau)}\cdot d\tilde{\mathbf{k}}(\tau) - i\Omega t'}, \quad (3)$$

where $\mathcal{A}_{\tilde{\mathbf{k}}} = \mathcal{A}^+_{\tilde{\mathbf{k}}} - \mathcal{A}^-_{\tilde{\mathbf{k}}}$ is the combined Berry connection between electron-hole pairs, $\mathcal{A}^\mu_{\tilde{\mathbf{k}}} = i\langle\mu, \tilde{\mathbf{k}}|\nabla_\mathbf{k}|\mu, \tilde{\mathbf{k}}\rangle$ is the Abelian Berry connection, $\mathbf{d}_{\tilde{\mathbf{k}}} = -ie\langle\psi_2^+(\tilde{\mathbf{k}})|\nabla_\mathbf{k}|\psi_1^-(\tilde{\mathbf{k}})\rangle$ is the instantaneous dipole moment, and $\delta E_{\tilde{\mathbf{k}}} = E^{2+}_{\tilde{\mathbf{k}}} - E^{1-}_{\tilde{\mathbf{k}}}$ is the energy of an electron-hole pair [72]. Then for an elliptically polarized THz field $\mathbf{F}(t) = F[\cos\theta\cos(\omega t), \sin\theta\sin(\omega t), 0]$, the optical response at $t_n = nT = 2n\pi/\omega$ explicitly contains the Berry phase $\phi_F^{(n)} = \int_0^{t_n}\mathcal{A}_{\tilde{\mathbf{k}}(\tau)}\cdot d\tilde{\mathbf{k}}(\tau)$, where the elliptical path $\tilde{\mathbf{k}}(t) = [k_x - k_0\cos\theta\sin(\omega t), k_y + k_0\sin\theta\cos(\omega t), k_z]$, $k_0 = eF/\omega$, and n is the number of completed cycles in $\mathbf{k}$ space (order of sidebands).

Now if the linearly polarized laser $\mathbf{E}_I = E\delta(t)\mathbf{e}_\parallel$ is applied in the x-y plane, then the dipole moment tensor $(\mathbf{d}^*_\mathbf{k}\mathbf{d}_\mathbf{k})^{t/b} = |d_{12}|^2[\mathbf{e}_x\mathbf{e}_x + \mathbf{e}_y\mathbf{e}_y \mp i(\mathbf{e}_x\mathbf{e}_y - \mathbf{e}_y\mathbf{e}_x)]$, which leads to opposite Berry phases on t and b as illustrated in Fig. 3(b). Thus the Faraday rotation of emission is

$$\phi_F^{(n)}(\theta) = n\int \mathcal{B}d\mathbf{k}^2, \quad (4)$$

where $\mathcal{B} = \sum_{i=1}^2 v_i^2\Delta_i/(\Delta_i^2 + v_i^2\mathbf{k}^2)^{3/2}$ is the Berry curvature. For an estimation, taking $v_1 \approx v_2 \approx 0.25$ eV nm, $\Delta_1 \approx 0.03$ eV, $\Delta_2 \approx 0.01$ eV, $\omega = 4$ meV, $F = 8$ kV cm^{-1}, and $k_0 = 0.2$ nm^{-1}. Then the estimated Faraday rotation angle is $\phi_1 \approx 3.5$ rad as in shown Fig. 3(c), which is surprisingly big due to giant Berry curvature from the small Dirac gap (two orders of magnitude larger than that in MoS_2 [72]).

The Faraday rotation from the Berry phase is robust as protected by $\mathcal{P}\Theta$. Moreover, without the elliptical THz field, the Faraday rotation in this material has to vanish due to $\mathcal{P}\Theta$. The resonant optical transitions from $\mathbf{E}_I$ will inevitably involve other trivial bulk states; however, without nontrivial Berry curvature in topological bands, these optical processes will not contribute to Faraday rotation. Even with possible large Berry curvature in bulk states, the much shorter lifetime of the bulk state [77] will hinder the phase accumulation of the electron-hole pairs, and thus contribute vanishingly small Faraday rotation. All of these provide a sharp experimental signature for the second SS. The Berry phase will only be slightly changed by taking into account the trigonal warping term. The Faraday rotation is also robust against the decoherence of electron-hole pairs due to scattering. However, to observe this effect, the layer coherence time needs to be longer than the period of the THz field. The SS on the two layers are physically decoupled, thus the layer coherence timescale is expected to be longer than that of electron-hole recombination.

C. Kerr effect in odd SL

In odd SL $MnBi_2Te_4$, $\mathcal{P}\Theta$ is broken due to an uncompensated magnetic layer. Therefore, the ac Hall conductance $\sigma_{xy}(\omega)$ is nonvanishing. In the limit of $\omega \to 0$, $\sigma_{xy}(0) = \pm e^2/h$ is the quantized anomalous Hall effect in transport [18]. Now the finite frequency $\sigma_{xy}(\omega)$ leads to the polar Kerr effect. For a thin film that is much thinner than the optical wavelength, the Kerr rotation angle $\theta_K = [8\pi/c(n^2 - 1)]\mathrm{Re}(\sigma_{xy})$ [41], where c is velocity of light and n is the refractive index of the substrate. The unoccupied topological

band associated with the second SS is a higher-energy replica of the band inversion that takes place near the Fermi energy. Transitions resonant with spin-orbit avoided band crossings are shown to make a large contribution to $\mathrm{Re}(\sigma_{xy})$ [78]. Therefore, similar to the resonant Kerr effect in magnetically doped TI [31], a resonant Kerr angle θ_K should occur at $\omega \approx 1.5$ eV in odd SL.

V. CONCLUSION

In summary, we present a model study of the unoccupied part of the band structure in $MnBi_2Te_4$. A possible second unoccupied topological SS is proposed which, if it exists, can be directly observed by 2PPE spectroscopy. We assume that such a second SS exists in $MnBi_2Te_4$ and further propose several optical experiments to reveal the second SS. Interestingly, due to direct optical coupling between these two SS, a giant Faraday rotation induced by the Berry curvature in second SS under strong THz fields can be observed in even SL through HSG. This proposal also applies to magnetic TI heterostructure [63,64]. These predictions, if experimentally realized, will show more efficient Faraday rotation by momentum space Berry curvature than traditional real space magnetic field, which may offer a unique opportunity for ultrafast optical device application without magnetic field. We hope the theoretical work here can motivate the study of higher-excited states in vast topological materials.

ACKNOWLEDGMENTS

This work is supported by the National Key Research Program of China under Grant No. 2019YFA0308404, the Natural Science Foundation of China through Grants No. 11774065 and No. 12174066, the Innovation Program for Quantum Science and Technology through Grant No. 2021ZD0302600, Shanghai Municipal Science and Technology Major Project under Grant No. 2019SHZDZX01, Science and Technology Commission of Shanghai Municipality under Grant No. 20JC1415900, and the Natural Science Foundation of Shanghai under Grant No. 19ZR1471400.

[1] C. L. Kane and E. J. Mele, Z_2 Topological Order and the Quantum Spin Hall Effect, Phys. Rev. Lett. **95**, 146802 (2005).
[2] C. L. Kane and E. J. Mele, Quantum Spin Hall Effect in Graphene, Phys. Rev. Lett. **95**, 226801 (2005).
[3] B. A. Bernevig, T. L. Hughes, and S.-C. Zhang, Quantum spin Hall effect and topological phase transition in HgTe quantum wells, Science **314**, 1757 (2006).
[4] M. König, S. Wiedmann, C. Brüne, A. Roth, H. Buhmann, L. Molenkamp, X.-L. Qi, and S.-C. Zhang, Quantum spin Hall insulator state in HgTe quantum wells, Science **318**, 766 (2007).
[5] M. Z. Hasan and C. L. Kane, *Colloquium*: Topological insulators, Rev. Mod. Phys. **82**, 3045 (2010).
[6] X.-L. Qi and S.-C. Zhang, Topological insulators and superconductors, Rev. Mod. Phys. **83**, 1057 (2011).
[7] D. Xiao, M.-C. Chang, and Q. Niu, Berry phase effects on electronic properties, Rev. Mod. Phys. **82**, 1959 (2010).
[8] Y. Tokura, K. Yasuda, and A. Tsukazaki, Magnetic topological insulators, Nat. Rev. Phys. **1**, 126 (2019).
[9] J. Wang and S.-C. Zhang, Topological states of condensed matter, Nat. Mater. **16**, 1062 (2017).
[10] L. Fu, C. L. Kane, and E. J. Mele, Topological Insulators in Three Dimensions, Phys. Rev. Lett. **98**, 106803 (2007).
[11] Y. Xia, D. Qian, D. Hsieh, L. Wray, A. Pal, H. Lin, A. Bansil, D. Grauer, Y. S. Hor, R. J. Cava, and M. Z. Hasan, Observation of a large-gap topological-insulator class with a single Dirac cone on the surface, Nat. Phys. **5**, 398 (2009).
[12] H. Zhang, C.-X. Liu, X.-L. Qi, X. Dai, Z. Fang, and S.-C. Zhang, Topological insulators in Bi_2Se_3, Bi_2Te_3 and Sb_2Te_3 with a single Dirac cone on the surface, Nat. Phys. **5**, 438 (2009).
[13] Y. L. Chen, J. G. Analytis, J.-H. Chu, Z. K. Liu, S.-K. Mo, X. L. Qi, H. J. Zhang, D. H. Lu, X. Dai, Z. Fang, S. C. Zhang, I. R. Fisher, Z. Hussain, and Z.-X. Shen, Experimental realization of a three-dimensional topological insulator, Bi_2Te_3, Science **325**, 178 (2009).
[14] P. Roushan, J. Seo, C. V. Parker, Y. S. Hor, D. Hsieh, D. Qian, A. Richardella, M. Z. Hasan, R. J. Cava, and A. Yazdani, Topological surface states protected from backscattering by chiral spin texture, Nature (London) **460**, 1106 (2009).
[15] A. R. Mellnik, J. S. Lee, A. Richardella, J. L. Grab, P. J. Mintun, M. H. Fischer, A. Vaezi, A. Manchon, E.-A. Kim, N. Samarth, and D. C. Ralph, Spin-transfer torque generated by a topological insulator, Nature (London) **511**, 449 (2014).
[16] X.-L. Qi, T. L. Hughes, and S.-C. Zhang, Topological field theory of time-reversal invariant insulators, Phys. Rev. B **78**, 195424 (2008).
[17] C.-Z. Chang, J. Zhang, X. Feng, J. Shen, Z. Zhang, M. Guo, K. Li, Y. Ou, P. Wei, L.-L. Wang, Z.-Q. Ji, Y. Feng, S. Ji, X. Chen, J. Jia, X. Dai, Z. Fang, S.-C. Zhang, K. He, Y. Wang *et al.*, Experimental observation of the quantum anomalous Hall effect in a magnetic topological insulator, Science **340**, 167 (2013).
[18] Y. Deng, Y. Yu, M. Z. Shi, Z. Guo, Z. Xu, J. Wang, X. H. Chen, and Y. Zhang, Quantum anomalous Hall effect in intrinsic magnetic topological insulator $MnBi_2Te_4$, Science **367**, 895 (2020).
[19] J. Maciejko, X.-L. Qi, H. D. Drew, and S.-C. Zhang, Topological Quantization in Units of the Fine Structure Constant, Phys. Rev. Lett. **105**, 166803 (2010).
[20] W.-K. Tse and A. H. MacDonald, Giant Magneto-Optical Kerr Effect and Universal Faraday Effect in Thin-Film Topological Insulators, Phys. Rev. Lett. **105**, 057401 (2010).
[21] L. Wu, M. Salehi, N. Koirala, J. Moon, S. Oh, and N. P. Armitage, Quantized Faraday and Kerr rotation and axion electrodynamics of a 3D topological insulator, Science **354**, 1124 (2016).
[22] K. N. Okada, Y. Takahashi, M. Mogi, R. Yoshimi, A. Tsukazaki, K. S. Takahashi, N. Ogawa, M. Kawasaki, and Y. Tokura, Terahertz spectroscopy on Faraday and Kerr rotations in a quantum anomalous Hall state, Nat. Commun. **7**, 12245 (2016).
[23] V. Dziom, A. Shuvaev, A. Pimenov, G. V. Astakhov, C. Ames, K. Bendias, J. Böttcher, G. Tkachov, E. M. Hankiewicz, C. Brüne, H. Buhmann, and L. W. Molenkamp, Observation of the universal magnetoelectric effect in a 3D topological insulator, Nat. Commun. **8**, 15197 (2017).

[24] M. Mogi, Y. Okamura, M. Kawamura, R. Yoshimi, K. Yasuda, A. Tsukazaki, K. S. Takahashi, T. Morimoto, N. Nagaosa, M. Kawasaki, Y. Takahashi, and Y. Tokura, Experimental signature of parity anomaly in semi-magnetic topological insulator, Nat. Phys. **18**, 390 (2022).

[25] X.-L. Qi, R. Li, J. Zang, and S.-C. Zhang, Seeing the magnetic monopole through the mirror of topological surface states, Science **323**, 1184 (2009).

[26] L. Fu and C. L. Kane, Superconducting Proximity Effect and Majorana Fermions at the Surface of a Topological Insulator, Phys. Rev. Lett. **100**, 096407 (2008).

[27] D. Hsieh, F. Mahmood, J. W. McIver, D. R. Gardner, Y. S. Lee, and N. Gedik, Selective Probing of Photoinduced Charge and Spin Dynamics in the Bulk and Surface of a Topological Insulator, Phys. Rev. Lett. **107**, 077401 (2011).

[28] Y. H. Wang, D. Hsieh, E. J. Sie, H. Steinberg, D. R. Gardner, Y. S. Lee, P. Jarillo-Herrero, and N. Gedik, Measurement of Intrinsic Dirac Fermion Cooling on the Surface of the Topological Insulator Bi_2Se_3 Using Time-Resolved and Angle-Resolved Photoemission Spectroscopy, Phys. Rev. Lett. **109**, 127401 (2012).

[29] D. Niesner, Th. Fauster, S. V. Eremeev, T. V. Menshchikova, Yu. M. Koroteev, A. P. Protogenov, E. V. Chulkov, O. E. Tereshchenko, K. A. Kokh, O. Alekperov, A. Nadjafov, and N. Mamedov, Unoccupied topological states on bismuth chalcogenides, Phys. Rev. B **86**, 205403 (2012).

[30] J. A. Sobota, S.-L. Yang, A. F. Kemper, J. J. Lee, F. T. Schmitt, W. Li, R. G. Moore, J. G. Analytis, I. R. Fisher, P. S. Kirchmann, T. P. Devereaux, and Z.-X. Shen, Direct Optical Coupling to an Unoccupied Dirac Surface State in the Topological Insulator Bi_2Se_3, Phys. Rev. Lett. **111**, 136802 (2013).

[31] S. Patankar, J. P. Hinton, Joel Griesmar, J. Orenstein, J. S. Dodge, X. Kou, L. Pan, K. L. Wang, A. J. Bestwick, E. J. Fox, D. Goldhaber-Gordon, J. Wang, and S.-C. Zhang, Resonant magneto-optic Kerr effect in the magnetic topological insulator $Cr : (Sb_x, Bi_{1-x})_2Te_3$, Phys. Rev. B **92**, 214440 (2015).

[32] D. Zhang, M. Shi, T. Zhu, D. Xing, H. Zhang, and J. Wang, Topological Axion States in the Magnetic Insulator $MnBi_2Te_4$ with the Quantized Magnetoelectric Effect, Phys. Rev. Lett. **122**, 206401 (2019).

[33] J. Li, Y. Li, S. Du, Z. Wang, B.-L. Gu, S.-C. Zhang, K. He, W. Duan, and Y. Xu, Intrinsic magnetic topological insulators in van der Waals layered $MnBi_2Te_4$-family materials, Sci. Adv. **5**, eaaw5685 (2019).

[34] Y. Gong, J. Guo, J. Li, K. Zhu, M. Liao, X. Liu, Q. Zhang, L. Gu, L. Tang, X. Feng, D. Zhang, W. Li, C. Song, L. Wang, P. Yu, X. Chen, Y. Wang, H. Yao, W. Duan, Y. Xu *et al.*, Experimental realization of an intrinsic magnetic topological insulator, Chin. Phys. Lett. **36**, 076801 (2019).

[35] M. M. Otrokov, I. I. Klimovskikh, H. Bentmann, A. Zeugner, Z. S. Aliev, S. Gass, A. U. B. Wolter, A. V. Koroleva, D. Estyunin, A. M. Shikin, M. Blanco-Rey, M. Hoffmann, A. Yu. Vyazovskaya, S. V. Eremeev, Y. M. Koroteev, I. R. Amiraslanov, M. B. Babanly, N. T. Mamedov, N. A. Abdullayev, V. N. Zverev *et al.*, Prediction and observation of an antiferromagnetic topological insulator, Nature (London) **576**, 416 (2019).

[36] Y.-Jie Hao, P. Liu, Y. Feng, X.-M. Ma, E. F. Schwier, M. Arita, S. Kumar, C. Hu, R. Lu, M. Zeng, Y. Wang, Z. Hao, H.-Y. Sun, K. Zhang, J. Mei, N. Ni, L. Wu, K. Shimada, C. Chen, Q. Liu *et al.*, Gapless Surface Dirac Cone in Antiferromagnetic Topological Insulator $MnBi_2Te_4$, Phys. Rev. X **9**, 041038 (2019).

[37] H. Li, S.-Y. Gao, S.-F. Duan, Y.-F. Xu, K.-J. Zhu, S.-J. Tian, J.-C. Gao, W.-H. Fan, Z.-C. Rao, J.-R. Huang, J.-J. Li, D.-Y. Yan, Z.-T. Liu, W.-L. Liu, Y.-B. Huang, Y.-L. Li, Y. Liu, G.-B. Zhang, P. Zhang, T. Kondo *et al.*, Dirac Surface States in Intrinsic Magnetic Topological Insulators $EuSn_2As_2$ and $MnBi_{2n}Te_{3n+1}$, Phys. Rev. X **9**, 041039 (2019).

[38] Y. J. Chen, L. X. Xu, J. H. Li, Y. W. Li, H. Y. Wang, C. F. Zhang, H. Li, Y. Wu, A. J. Liang, C. Chen, S. W. Jung, C. Cacho, Y. H. Mao, S. Liu, M. X. Wang, Y. F. Guo, Y. Xu, Z. K. Liu, L. X. Yang, and Y. L. Chen, Topological Electronic Structure and Its Temperature Evolution in Antiferromagnetic Topological Insulator $MnBi_2Te_4$, Phys. Rev. X **9**, 041040 (2019).

[39] P. Swatek, Y. Wu, L.-L. Wang, K. Lee, B. Schrunk, J. Yan, and A. Kaminski, Gapless Dirac surface states in the antiferromagnetic topological insulator $MnBi_2Te_4$, Phys. Rev. B **101**, 161109(R) (2020).

[40] J.-Q. Yan, Q. Zhang, T. Heitmann, Z. Huang, K. Y. Chen, J.-G. Cheng, W. Wu, D. Vaknin, B. C. Sales, and R. J. McQueeney, Crystal growth and magnetic structure of $MnBi_2Te_4$, Phys. Rev. Materials **3**, 064202 (2019).

[41] See Supplemental Material at http://link.aps.org/supplemental/10.1103/PhysRevB.106.045148 for technical details.

[42] G. Kresse and J. Furthmüller, Efficient iterative schemes for *ab initio* total-energy calculations using a plane-wave basis set, Phys. Rev. B **54**, 11169 (1996).

[43] P. E. Blöchl, Projector augmented-wave method, Phys. Rev. B **50**, 17953 (1994).

[44] J. P. Perdew, K. Burke, and M. Ernzerhof, Generalized Gradient Approximation Made Simple, Phys. Rev. Lett. **77**, 3865 (1996).

[45] S. Grimme, J. Antony, S. Ehrlich, and H. Krieg, A consistent and accurate *ab initio* parametrization of density functional dispersion correction (DFT-D) for the 94 elements H-Pu, J. Chem. Phys. **132**, 154104 (2010).

[46] S. L. Dudarev, G. A. Botton, S. Y. Savrasov, C. J. Humphreys, and A. P. Sutton, Electron-energy-loss spectra and the structural stability of nickel oxide: An LSDA+U study, Phys. Rev. B **57**, 1505 (1998).

[47] A. A. Mostofi, J. R. Yates, Y.-S. Lee, I. Souza, D. Vanderbilt, and N. Marzari, Wannier9: A tool for obtaining maximally-localised Wannier functions, Comput. Phys. Commun. **178**, 685 (2008).

[48] QuanSheng Wu, ShengNan Zhang, H.-F. Song, M. Troyer, and A. A. Soluyanov, Wanniertools: An open-source software package for novel topological materials, Comput. Phys. Commun. **224**, 405 (2018).

[49] J. Gao, Q. Wu, C. Persson, and Z. Wang, Irvsp: To obtain irreducible representations of electronic states in the VASP, Comput. Phys. Commun. **261**, 107760 (2021).

[50] M. Shishkin and G. Kresse, Implementation and performance of the frequency-dependent *GW* method within the PAW framework, Phys. Rev. B **74**, 035101 (2006).

[51] M. Shishkin, M. Marsman, and G. Kresse, Accurate Quasiparticle Spectra from Self-Consistent *GW* Calculations with Vertex Corrections, Phys. Rev. Lett. **99**, 246403 (2007).

[52] F. Fuchs, J. Furthmüller, F. Bechstedt, M. Shishkin, and G. Kresse, Quasiparticle band structure based on a generalized Kohn-Sham scheme, Phys. Rev. B **76**, 115109 (2007).

[53] I. Aguilera, C. Friedrich, G. Bihlmayer, and S. Blügel, *GW* study of topological insulators Bi_2Se_3, Bi_2Te_3, and Sb_2Te_3: Beyond the perturbative one-shot approach, Phys. Rev. B **88**, 045206 (2013).

[54] P. Aguado-Puente, S. Fahy, and M. Grüning, *GW* study of pressure-induced topological insulator transition in group-IV tellurides, Phys. Rev. Research **2**, 043105 (2020).

[55] T. Förster, P. Krüger, and M. Rohlfing, Two-dimensional topological phases and electronic spectrum of Bi_2Se_3 thin films from *GW* calculations, Phys. Rev. B **92**, 201404(R) (2015).

[56] D. Y. Qiu, F. H. da Jornada, and S. G. Louie, Optical Spectrum of MoS_2: Many-Body Effects and Diversity of Exciton States, Phys. Rev. Lett. **111**, 216805 (2013).

[57] S. Grimme, Semiempirical GGA-type density functional constructed with a long-range dispersion correction, J. Comput. Chem. **27**, 1787 (2006).

[58] R. S. K. Mong, A. M. Essin, and J. E. Moore, Antiferromagnetic topological insulators, Phys. Rev. B **81**, 245209 (2010).

[59] L. Fu and C. L. Kane, Topological insulators with inversion symmetry, Phys. Rev. B **76**, 045302 (2007).

[60] L. Fu, Hexagonal Warping Effects in the Surface States of the Topological Insulator Bi_2Te_3, Phys. Rev. Lett. **103**, 266801 (2009).

[61] J. Wang, B. Lian, and S.-C. Zhang, Universal scaling of the quantum anomalous Hall plateau transition, Phys. Rev. B **89**, 085106 (2014).

[62] J. Wang, B. Lian, X.-L. Qi, and S.-C. Zhang, Quantized topological magnetoelectric effect of the zero-plateau quantum anomalous Hall state, Phys. Rev. B **92**, 081107(R) (2015).

[63] M. Mogi, M. Kawamura, R. Yoshimi, A. Tsukazaki, Y. Kozuka, N. Shirakawa, K. S. Takahashi, M. Kawasaki, and Y. Tokura, A magnetic heterostructure of topological insulators as a candidate for an axion insulator, Nat. Mater. **16**, 516 (2017).

[64] D. Xiao, J. Jiang, J.-H. Shin, W. Wang, F. Wang, Y.-F. Zhao, C. Liu, W. Wu, M. H. W. Chan, N. Samarth, and C.-Z. Chang, Realization of the Axion Insulator State in Quantum Anomalous Hall Sandwich Heterostructures, Phys. Rev. Lett. **120**, 056801 (2018).

[65] C. Liu, Y. Wang, H. Li, Y. Wu, Y. Li, J. Li, K. He, Y. Xu, J. Zhang, and Y. Wang, Robust axion insulator and Chern insulator phases in a two-dimensional antiferromagnetic topological insulator, Nat. Mater. **19**, 522 (2020).

[66] K. Nomura and N. Nagaosa, Surface-Quantized Anomalous Hall Current and the Magnetoelectric Effect in Magnetically Disordered Topological Insulators, Phys. Rev. Lett. **106**, 166802 (2011).

[67] J. Yu, J. Zang, and C.-X. Liu, Magnetic resonance induced pseudoelectric field and giant current response in axion insulators, Phys. Rev. B **100**, 075303 (2019).

[68] Z. Liu and J. Wang, Anisotropic topological magnetoelectric effect in axion insulators, Phys. Rev. B **101**, 205130 (2020).

[69] Z. Liu, J. Xiao, and J. Wang, Dynamical magnetoelectric coupling in axion insulator thin films, Phys. Rev. B **105**, 214424 (2022).

[70] R.-B. Liu and B.-F. Zhu, High-order THz-sideband generation in semiconductors, in *AIP Conference Proceedings* (American Institute of Physics, 2007), Vol. 893, pp. 1455–1456.

[71] B. Zaks, R.-B. Liu, and M. S. Sherwin, Experimental observation of electron–hole recollisions, Nature (London) **483**, 580 (2012).

[72] F. Yang and R.-B. Liu, Berry phases of quantum trajectories of optically excited electron–hole pairs in semiconductors under strong terahertz fields, New J. Phys. **15**, 115005 (2013).

[73] F. Yang, X. Xu, and R.-B. Liu, Giant Faraday rotation induced by the Berry phase in bilayer graphene under strong terahertz fields, New J. Phys. **16**, 043014 (2014).

[74] H. B. Banks, Q. Wu, D. C. Valovcin, S. Mack, A. C. Gossard, L. Pfeiffer, R.-B. Liu, and M. S. Sherwin, Dynamical Birefringence: Electron-Hole Recollisions as Probes of Berry Curvature, Phys. Rev. X **7**, 041042 (2017).

[75] F. Langer, C. P. Schmid, S. Schlauderer, M. Gmitra, J. Fabian, P. Nagler, C. Schuller, T. Korn, P. G. Hawkins, J. T. Steiner, U. Huttner, S. W. Koch, M. Kira, and R. Huber, Lightwave valleytronics in a monolayer of tungsten diselenide, Nature (London) **557**, 76 (2018).

[76] D. Xiao, G.-B. Liu, W. Feng, X. Xu, and W. Yao, Coupled Spin and Valley Physics in Monolayers of MoS_2 and Other Group-VI Dichalcogenides, Phys. Rev. Lett. **108**, 196802 (2012).

[77] J. A. Sobota, S. Yang, J. G. Analytis, Y. L. Chen, I. R. Fisher, P. S. Kirchmann, and Z.-X. Shen, Ultrafast Optical Excitation of a Persistent Surface-State Population in the Topological Insulator Bi_2Se_3, Phys. Rev. Lett. **108**, 117403 (2012).

[78] Z. Fang, K. Terakura, and N. Nagaosa, Orbital physics in ruthenates: First-principles studies, New J. Phys. **7**, 66 (2005).